Report No. 29 Jan. 31, 2001

SIMULATION OF E-BEAM TRANSPORT AND STEERING IN THE H.V. TERMINAL

D. Bar-Lev, I. Merhasin, A. Gover, Y. Pinhasi

The purpose of this report is to verify that the quads and steering coils in the HV terminal can transport and steer the e-beam so that there is little likelihood for electron interception in the apertures. The main result reported is Table 4 suggesting two sets of quad excitation currents recommended for optimal beam transport.

Numerical simulations were carried out with the new version of EL-OP (Jan. 2001) which includes a correction of an earlier error in computation of electron trajectories (reversibility).

The new location of the steering coils and quads which were reset after the relocation of the wiggler and resonator are described in Figs. 1,2 and Table 1.

1. Propagation through the wiggler of the beam center electron-trajectory

The wiggler model parameters (including the correction magnets) are given in Table 2. (see report no. 2-4/97 for parameter definitions)

Based on theoretical calculation, the wiggling amplitude (not considering the long magnets) is:

$$X_w = \frac{eB_w}{v_z \gamma m k_w^2} = 1.6466\text{mm}$$

Because of the simmetry at the wiggler, we choose the coordinates of the beam center electron a $z = 0$ to be: $X(0) = -X_w = -1.6466$mm, $\alpha_x(0) = 0$, $y(0)=0$, $\alpha_y(0)=0$.

For this value it was possible to propagate the electron inside the wiggler along the wiggler axis without betatron oscillations.

The values of the correction magnets were modified (in a symmetric way) to verify that the beam – center electron trajectory out of the wiggler stays on axis on both sides of the wiggler (these values may be slightly different from the real life values – the steering coils are expected to correct deviation of the beam center trajectory in real life).

The ideal beam-center electron trajectory is shown in Figs. 3a,b.

2. Steering Coils

Our first concern was to verify that steering coil relocated VH6 has enough leverage to steer the e-beam across the exit aperture of the resonator (diameter – 10 mm). Also the combination VH6-VH7 should be able to steer the beam center (in angle and displacement) and place it on the accelerator axis even if there are small deviations of the beam trajectory off the wiggler axis. These tests were carried out by running EL-OP with the permanent magnet models of the steering coils.

The EL-OP model of steering coils VH6 VH7 are given in Table 3:

Fig. 4 describes the steering limits of VH6. For maximum coil current limits ±3A the maximum displacement at the resonator aperture plane is:

Table 1: Location of components and apertures

Object	Distance from Cathode [mm]	Distance from wiggler's center [mm]
Q_1	4071	- 2132
Q_2	4761	- 1787
Q_3	5106	- 1442
Q_4	5451	- 1097
Q_5	7645	1097
Q_6	7990	1442
Q_7	8335	1787
Q_8	8680	2132
VH_6	7137	589
VH_7	7493	945
Entrance aperture	5902	-646
Exit aperture	7219	671

Notice the full symmetry of the quad positions with respective to the wiggler center. The entrance and the exit apertures are situated almost symmetrically (exact symmetric positioning was not possible because of mechanical constraints).

$\Delta X = \pm 1.6$mm
$\Delta Y = \pm 5$mm

The maximum angular deviation is

$\Delta\alpha_x = 31.3$ mrad $\quad (\Delta\alpha_x/\Delta I = 10.43$ mrad/A)
$\Delta\alpha_y = 66.9$ mrad $\quad (\Delta\alpha_y/\Delta I = 22.3$ mrad/A)

The displacement $\Delta X = \pm 1.6$mm is not big as we would like. The overlap of the coil and wiggler magnetic fields limits the steering.

Fig. 5 describes the maximum deviation in x and y dimensions that steering coil VH7 can correct. For maximum coil excitation currents ±3A, VH7 can correct trajectories emanating from the aperture plane (z = 671mm) with

$\Delta X = \Delta Y = \pm 22$mm

$\Delta\alpha_x = \Delta\alpha_y = 79.35$ mrad $\qquad (\Delta\alpha/\Delta I = 26.45$ mrad/A)

Clearly, this is enough.

Fig. 1: Location of main Electron Optical Components in the Terminal

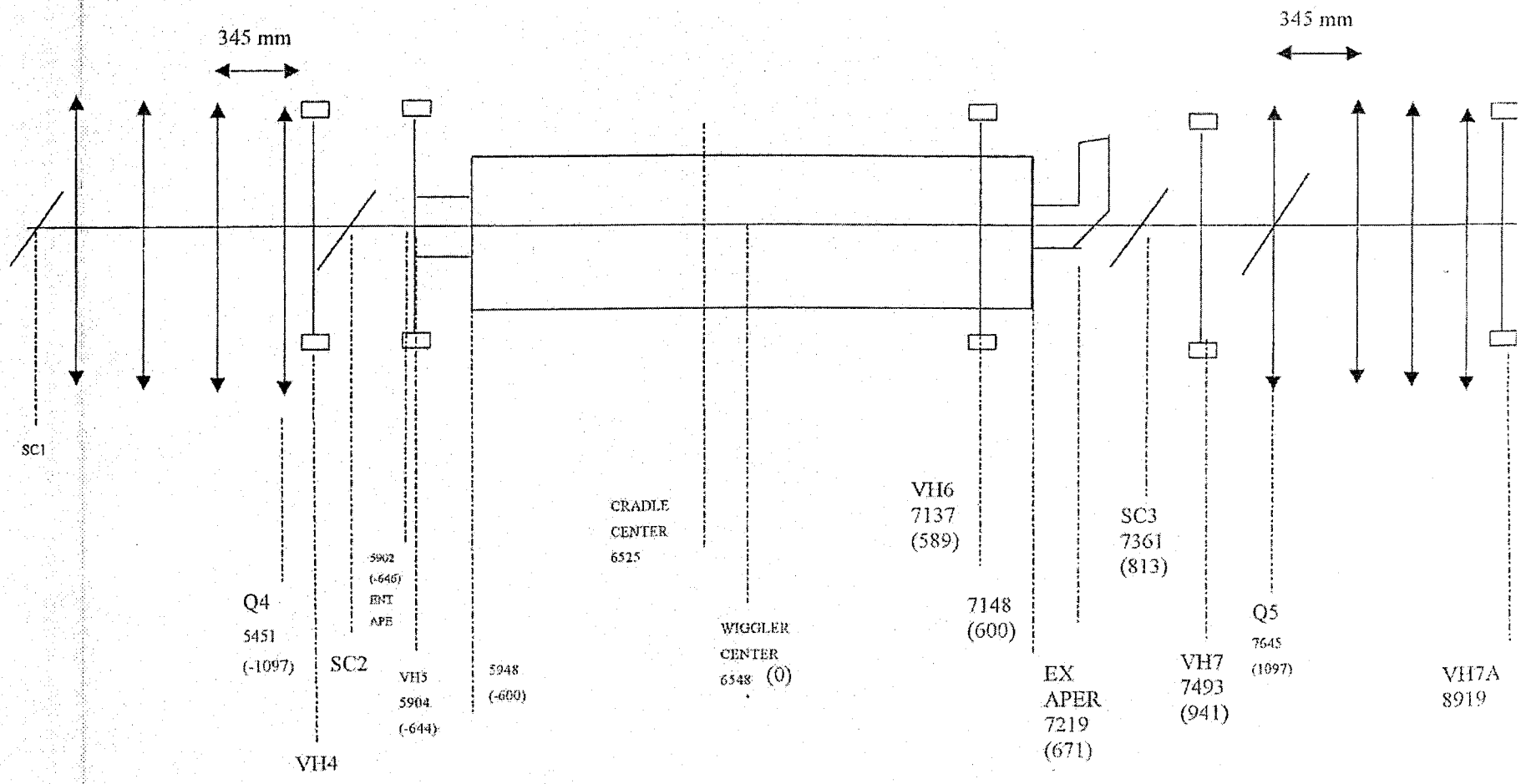

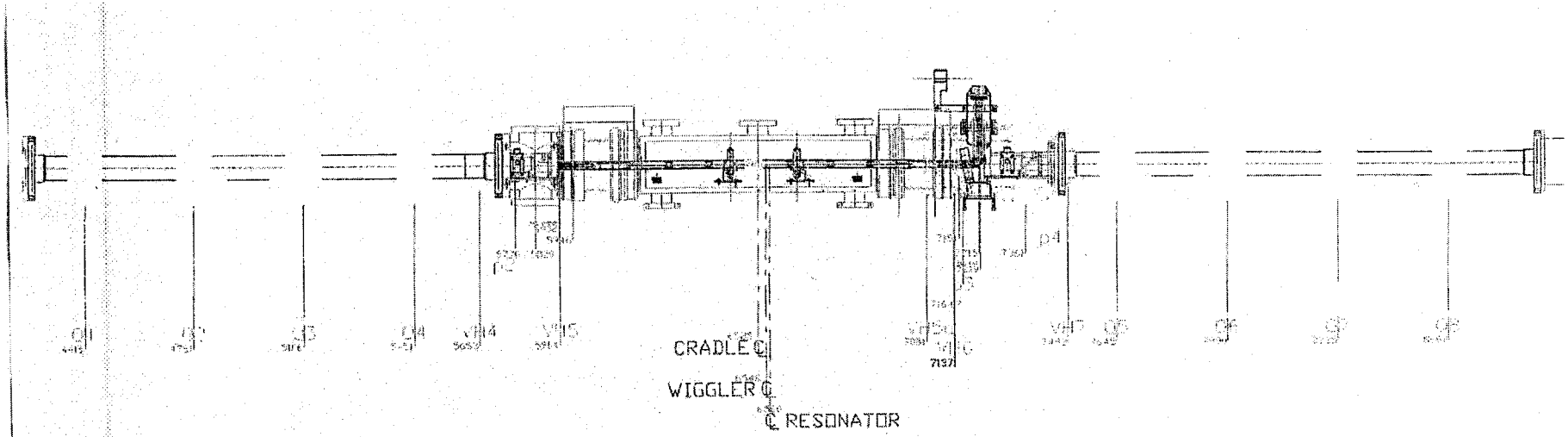

Fig. 9

system configuration
- [x] Wiggler
- [x] Entrance/Exit Magnets
- [x] Focusing Quads
- [ ] Focusing Coils
- [ ] Additional Coils
- [ ] Additional Steer. Coils

Electron Energy, kEv: 1400

[ ] Space Charge

Electron current, Amp: 1

magnet dimensions, mm
- 50.8 a0
- 11.11 b0
- 11.11 c0

Long Magnets

magnet dimensions, mm
- 11.11 al
- 11.11 bl
- 1201.4 cl

Saturating Field, Gs
- 8094 Bs0

Saturating Field, Gs
- 8480 Bsl

wiggler properties
- 26 number of periods
- 6 periods account for
- 25 gap, mm

magnet positions, mm
- 0 z0
- 28.25 dl

resonator properties
- -600 left end position, mm
- 600 rigth end position, mm
- 11 resonator width, mm

working frequency
- 26 GHz

Entrance magnet pairs: 2

	a	b	c	d	l	alpha	Bs
1	50.8	11.11	5.55	18.6	19.94	180	9498
2	50.8	11.11	5.55	35.8	11.11	-90	9498

Exit magnet pairs: 3

	a	b	c	d	l	alpha	Bs
1	50.8	11.11	11.11	18.05	11.11	0	8094
2	50.8	11.11	5.55	35.8	22.22	90	9498
3	50.8	11.11	5.55	18.6	31.05	180	9498

Table 2: Wiggler's parameters

Fig. 3a: Trajectory of center beam electron

- notice the lack of "betatron oscillation"

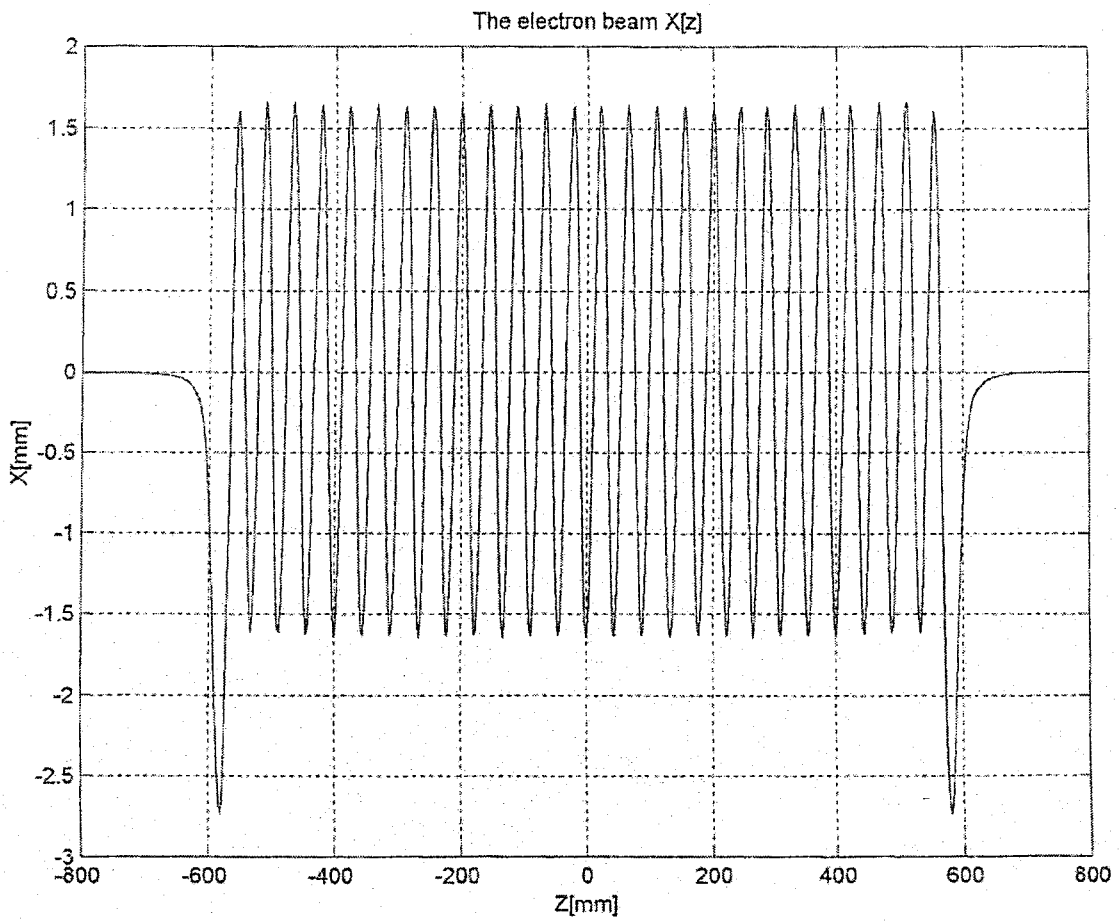

Fig. 3b: Three Dimensional Trajectory

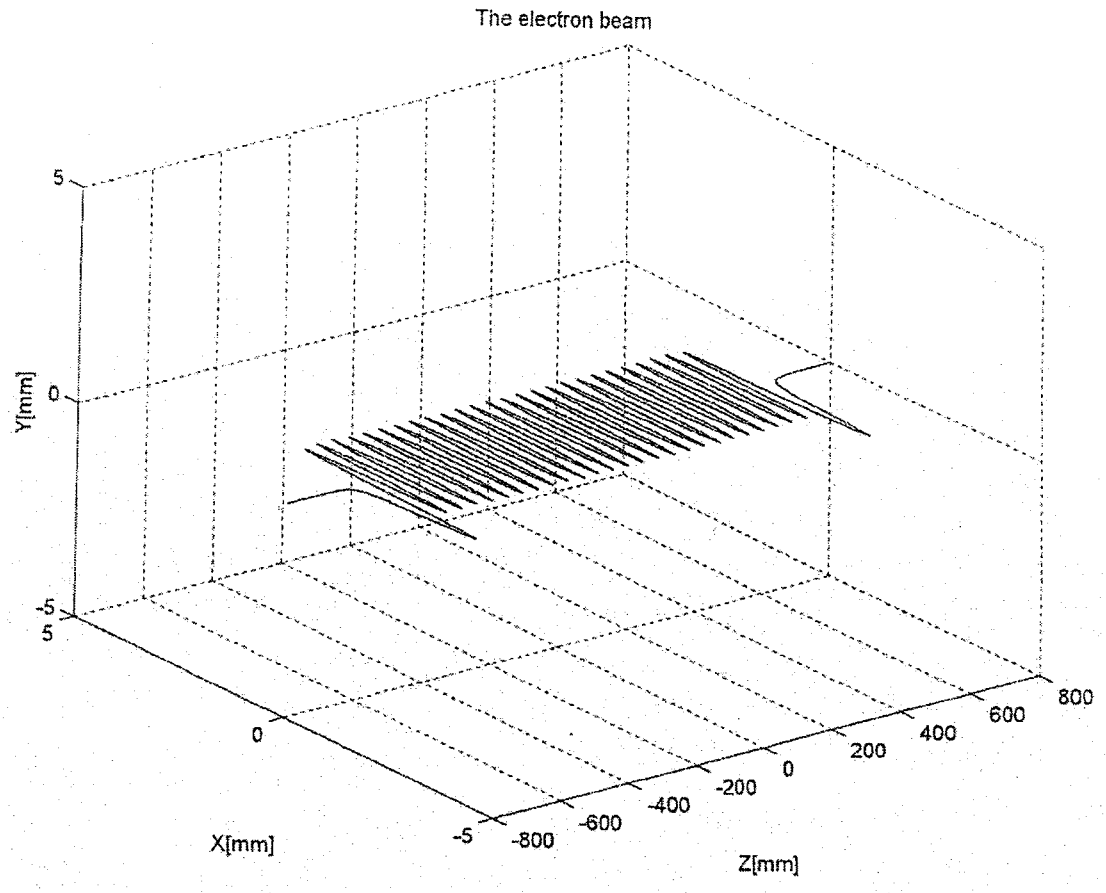

Table 3: ELOP model of steering coils VH6, VH7

	a	b	c	Xm	Ym	Zm	alpha	betha	Bs	Type	Bs/IA
	12	159	12	85.5	0	589	0	0	0	H6	2184
	12	159	12	-85.5	0	589	0	0	0	H6	2184
	183	12	12	0	85.5	589	180	0	0	H6	139
	183	12	12	0	-85.5	589	180	0	0	H6	139
	183	12	12	85.5	0	589	0	-90	0	V6	139
	183	12	12	-85.5	0	589	0	-90	0	V6	139
	12	159	12	0	85.5	589	0	90	0	V6	2184
	12	159	12	0	-85.5	589	0	90	0	V6	2184
	11	101.5	11	56.25	0	945	0	0	-6525.	H7	2175.
	11	101.5	11	-56.25	0	945	0	0	-6525.	H7	2175.
	123.5	11	11	0	56.25	945	180	0	-813.5	H7	271.1
	123.5	11	11	0	-56.25	945	180	0	-813.5	H7	271.1
	123.5	11	11	0	-56.25	945	180	0	-813.5	H7	271.1
	101.5	11	11	56.25	0	945	0	-90	-813.5	V7	271.1
	101.5	11	11	-56.25	0	945	0	-90	-813.5	V7	271.1
	11	123.5	11	0	56.25	945	0	90	-6525.	V7	2175.
	11	123.5	11	0	-56.25	945	0	90	-6525.	V7	2175.

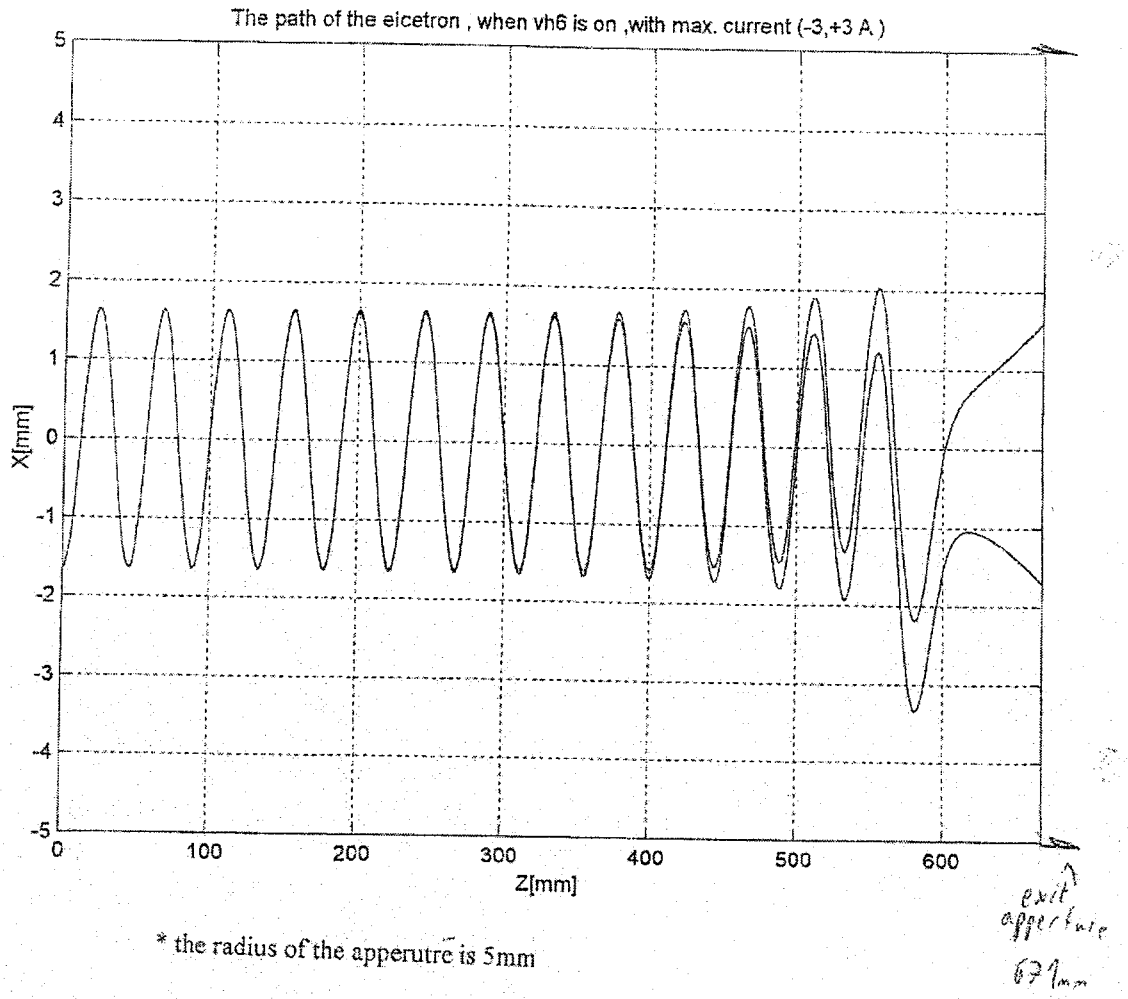

* the radius of the apperutre is 5mm

Fig. 4a: Maximum steering of VH6 in X-dimension

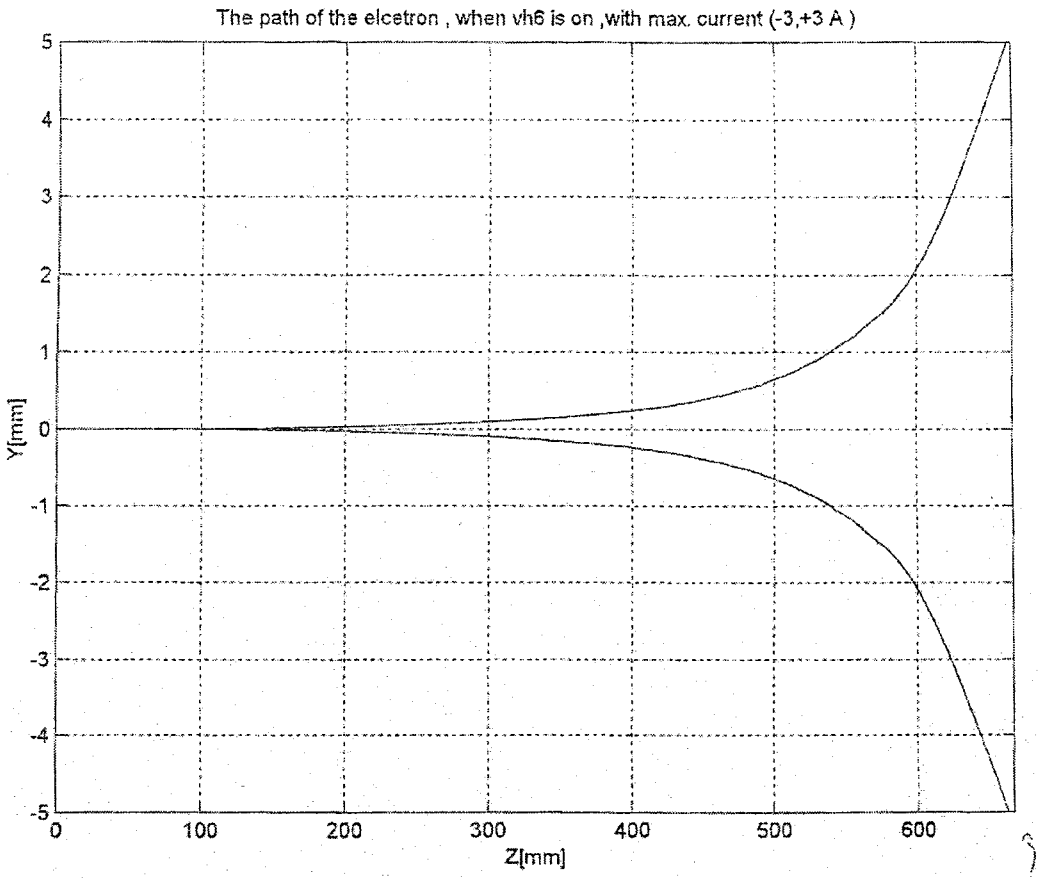

* the radius of the upper lare is 5mm.

exit aperture
671mm

Fig. 4b: Maximum steering of VH6 in Y-dimension

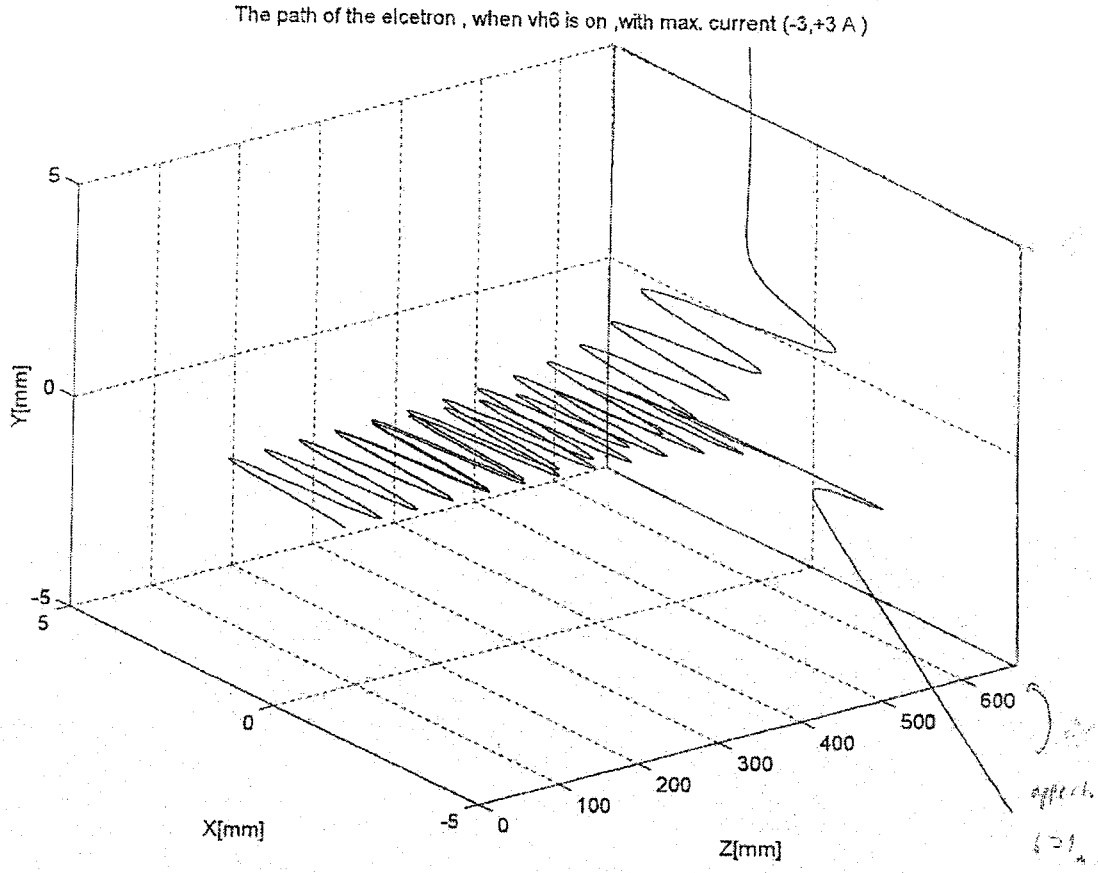

Fig. 4c: Three Dimensional Trajectories (VH6)

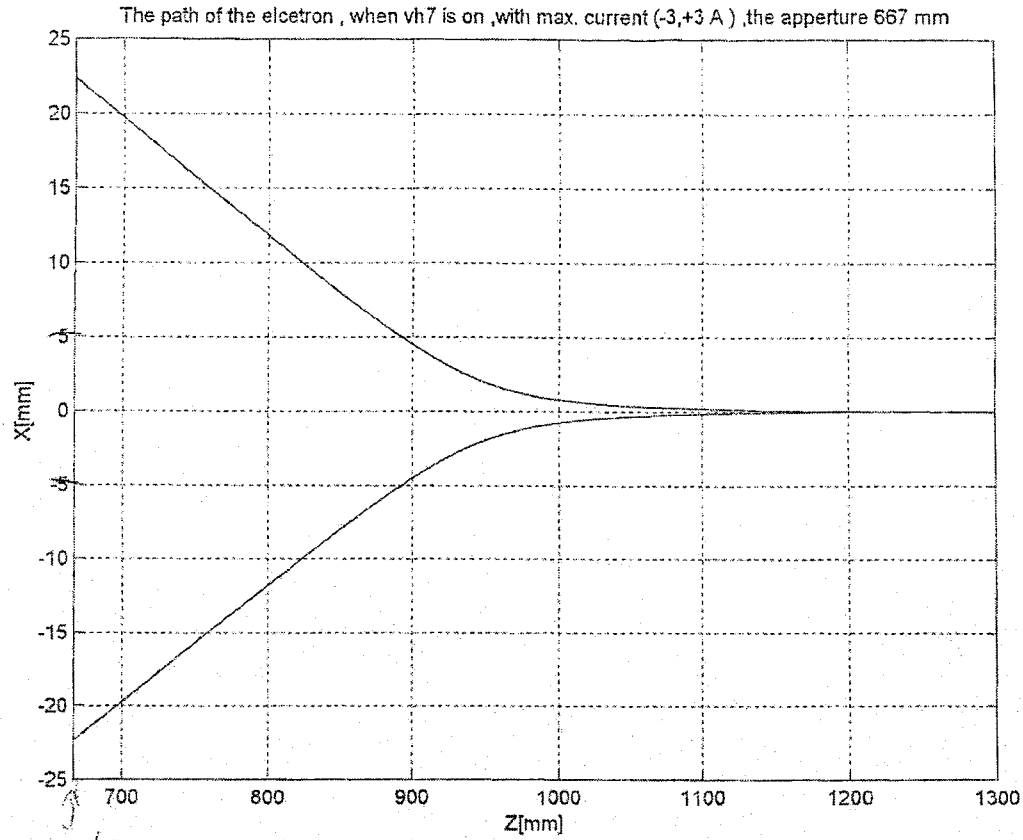

Fig. 5a: Maximum steering of VH7 in X – dimension

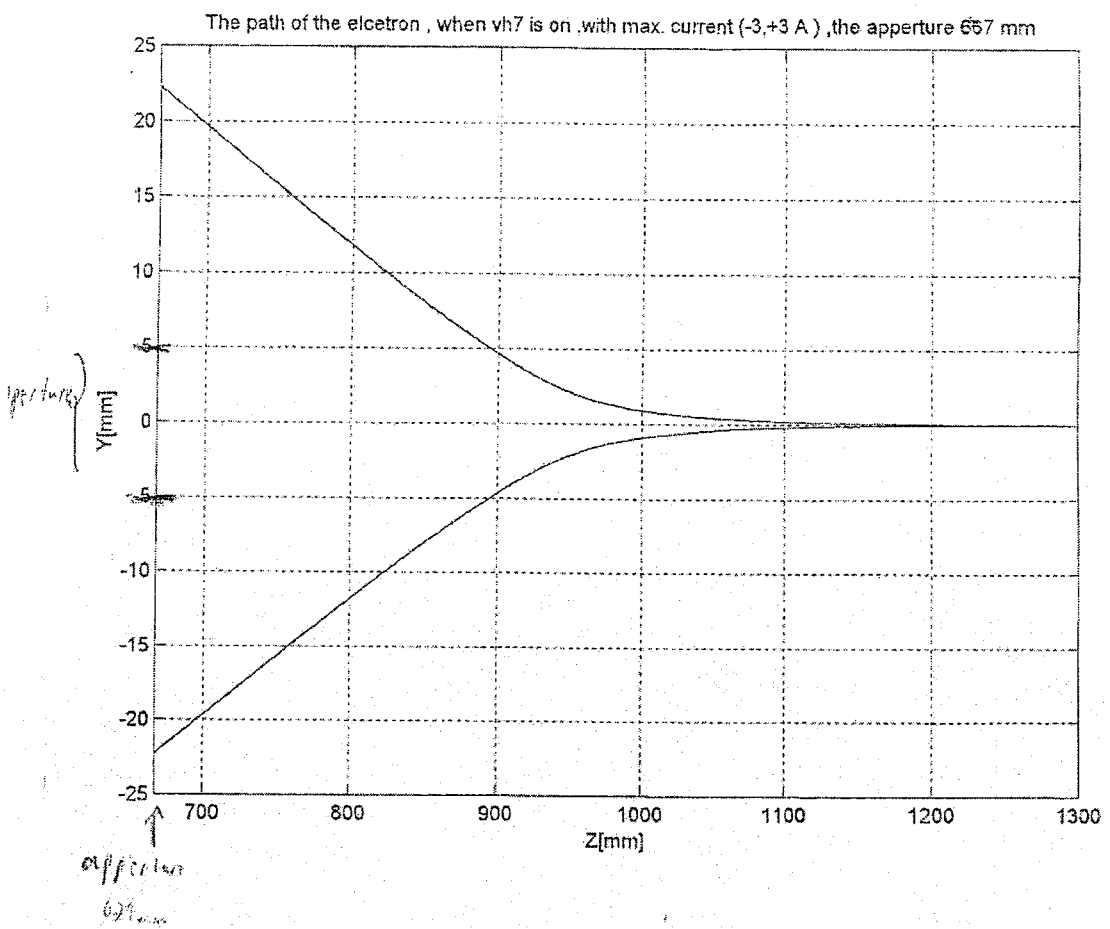

Fig. 5b: Maximum steering of VH7 in Y – dimension

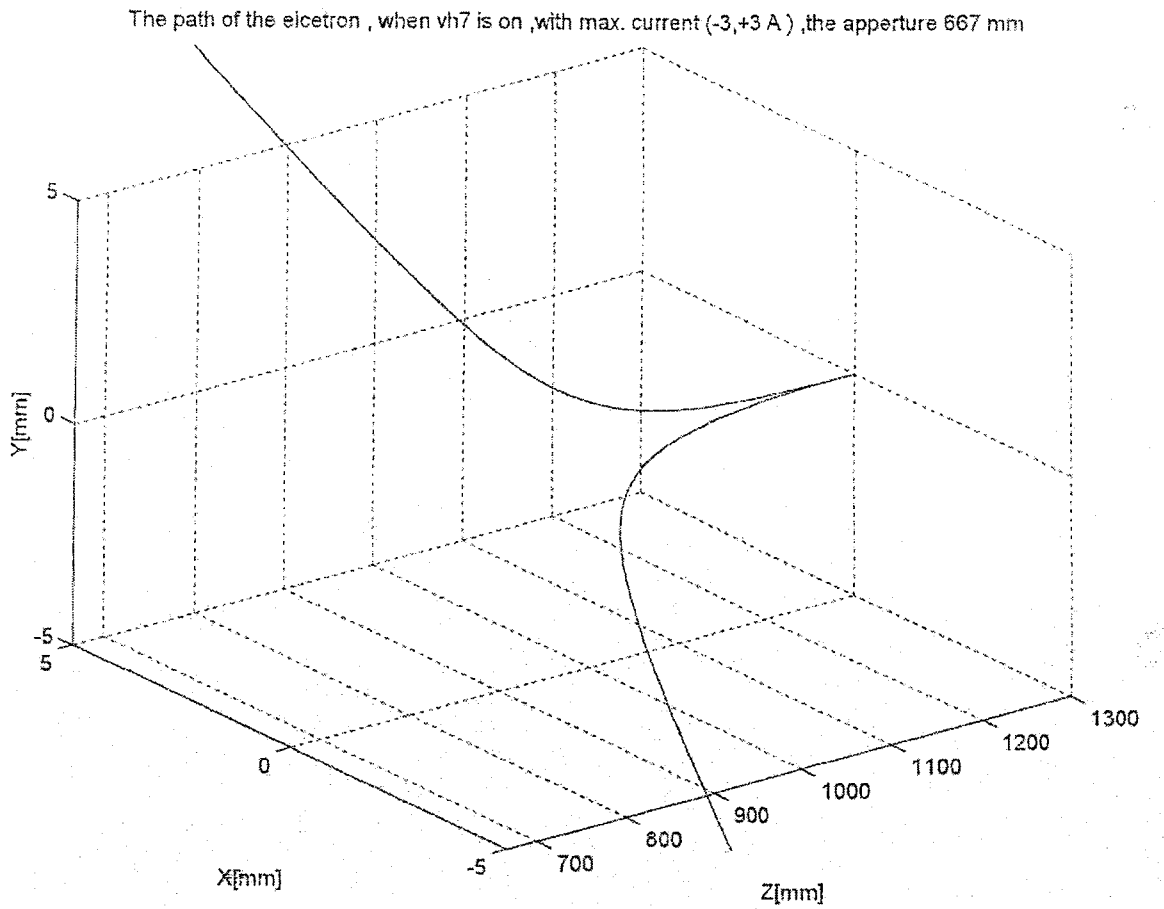

Fig. 5c: Three Dimensional Plot (VH7)

3. E-Beam propagation in the wiggler

For optimal propagation of the e-beam through the wiggler (no scalloping), we ran EL-OP with 59 particles for an elliptical beam distribution in phase space.

The beam transport starts at z = 0 where we assume in phase spaces (x, α_x) (y, α_y) elipses centered around the beam center electron trajectory coordinates, $\alpha_x(0) = 0$, x(0)=-1.6466mm, (y(0) = 0, $\alpha_y(0) = 0$). The optimal beam radiuses which were used as the horizontal radii of the phase-space ellipses in EL-OP input file were determined from the theoretical formulae:

$$X_b = \sqrt{\frac{\varepsilon}{\pi k_{bx}}} = 1.00305\text{mm}$$

$$Y_b = \sqrt{\frac{\varepsilon}{\pi k_{by}}} = 1.574\text{mm}$$

The numerical values were computed for the parameters:
$\varepsilon = 22\pi$ mm mrad
$k_{bx} = 21.87$ rad/m
$k_{by} = 8.8798$ rad/m

Figs. 6 a,b display beam propagation in the wiggler in the x and y dimensions respectively. The beam was propagated from z=0 in the positive and negative z directions and the trajectory files of the two runs were combined into one drawing. The propagation is almost scallop-free.
The beam widths at the resonator aperture locations are:
2X(-646) ≅ 2X(671) ≅3.6 mm
2Y(-646) ≅ 2Y(671) ≅ 6.0 mm
The aperture is 10mm diameter, so if the beam transverse distribution does not have much "tail" or "hollow" the beam will go through the apertures.

Fig. 6a:

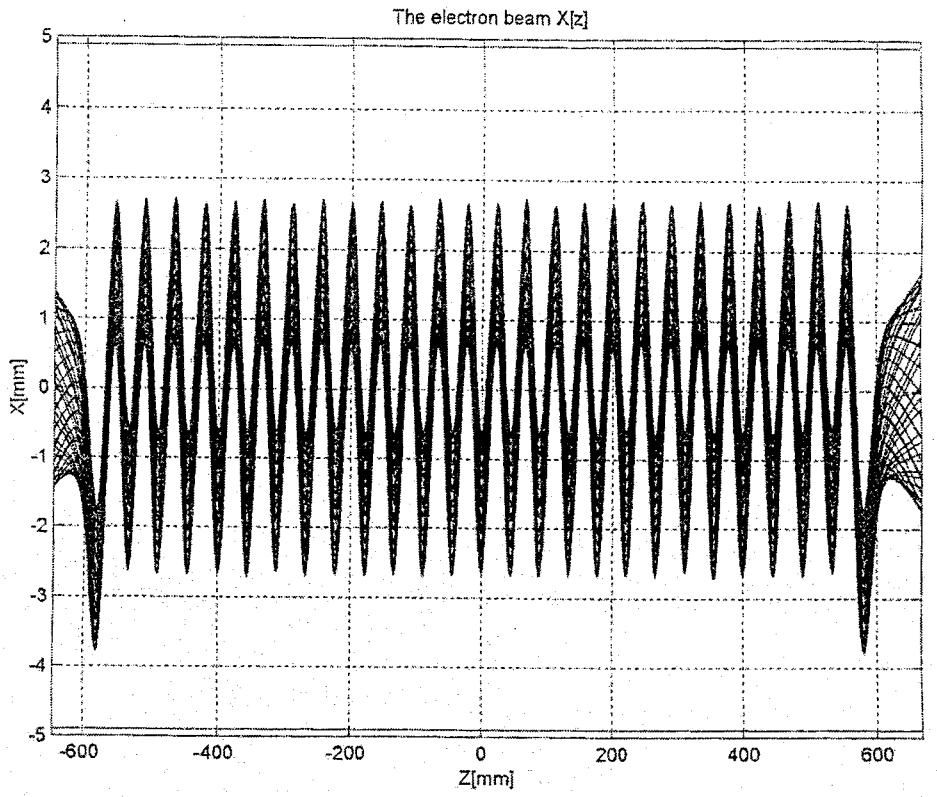

- notice the lack of scalloping

Fig. 6b:

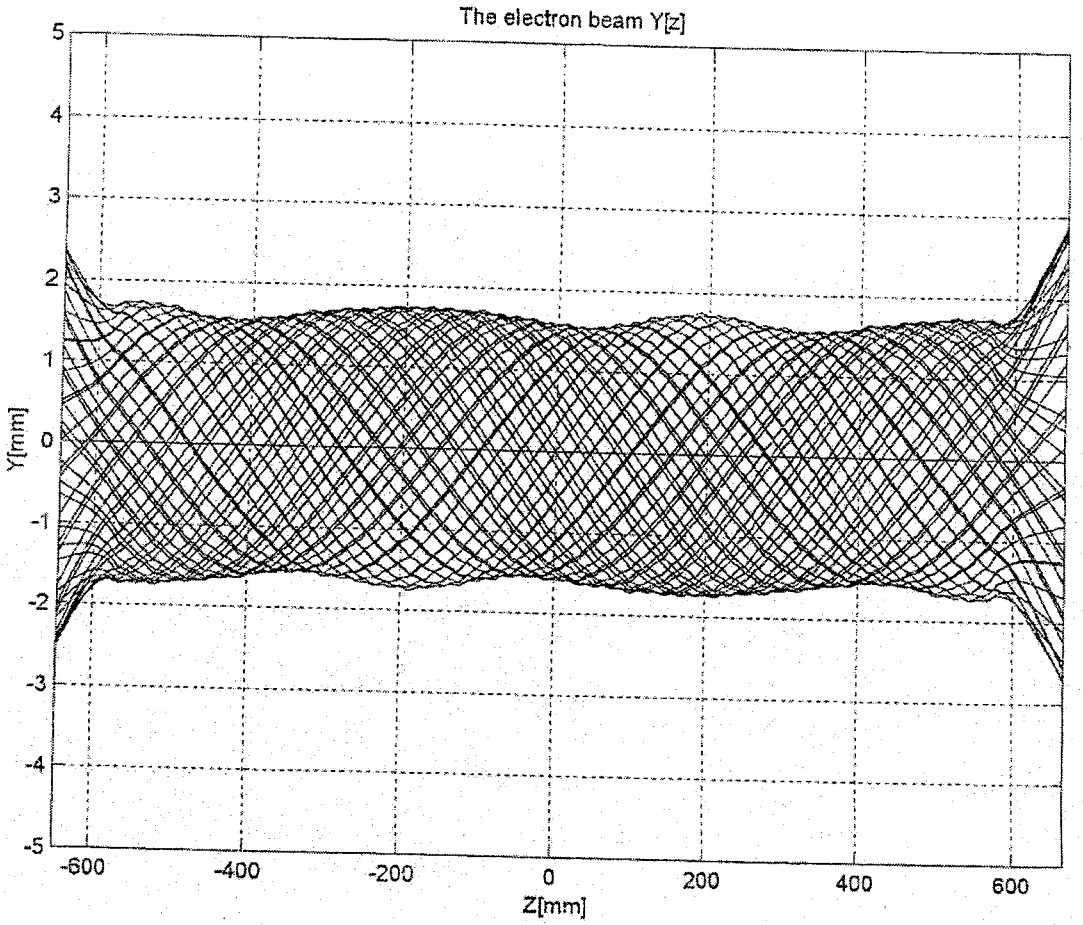

- notice the relatively small scalloping

4. Finding the Beam Virtual Waists

The directions of the electron trajectories of the beam far away from the wiggler exit (z = 800), were reversed, and the beam was propagated backward with the wiggler magnet fields "extinguished". This revealed the position and waist sizes of the virtual beam-waist on the exit side (Fig. 7 a-d). A similar process was carried out on the entrance side (Fig. 7 e,f).

From those figures we determined the virtual waist positions and waist sizes:

$Z_{wy} = \pm 537$ mm
$2W_{y0} = 2.35$ mm
$Z_{wx} = \pm 600$ mm
$2W_{x0} = 2.23$ mm

Fig. 7a: Wiggler's focus Y-dimension at the wiggler exit

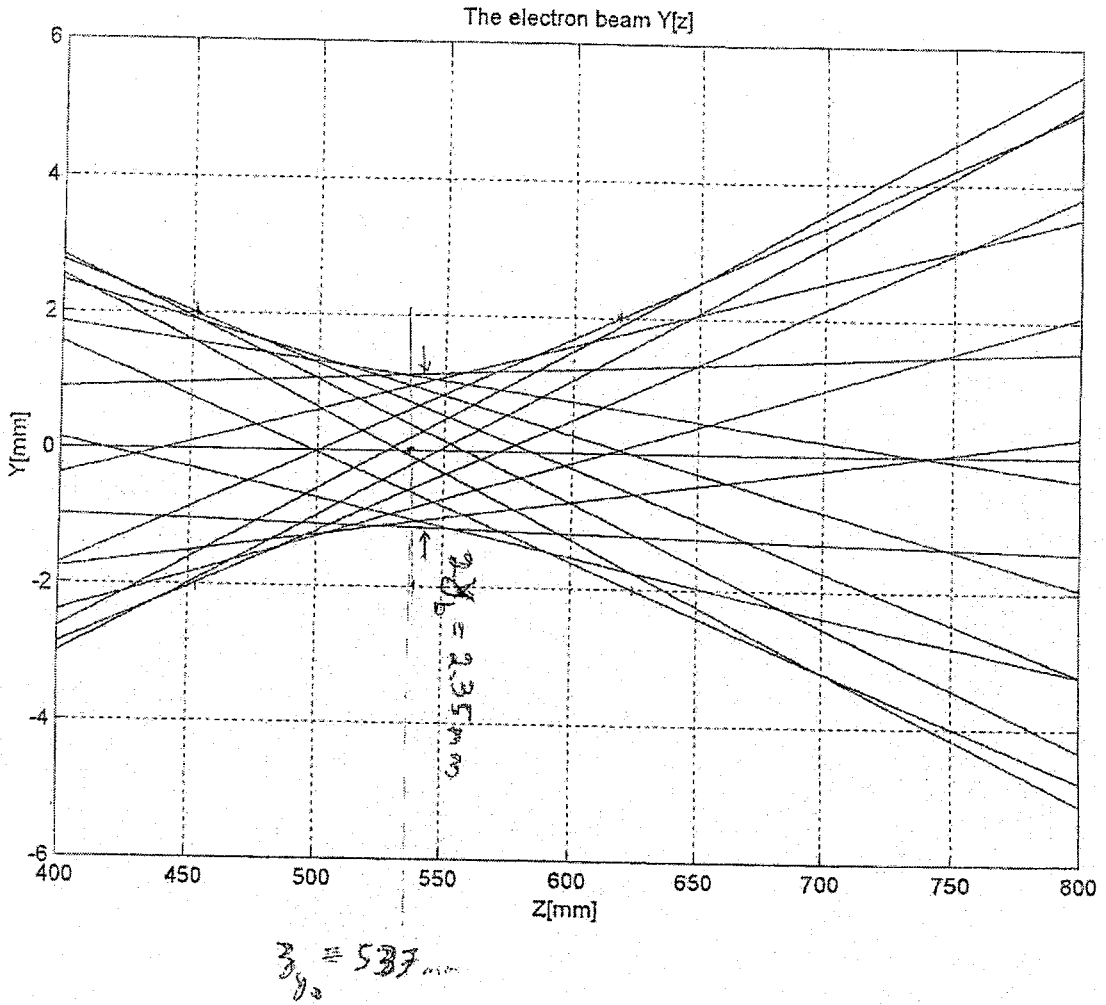

Fig. 7b: Larger scale (Wiggler's focus)

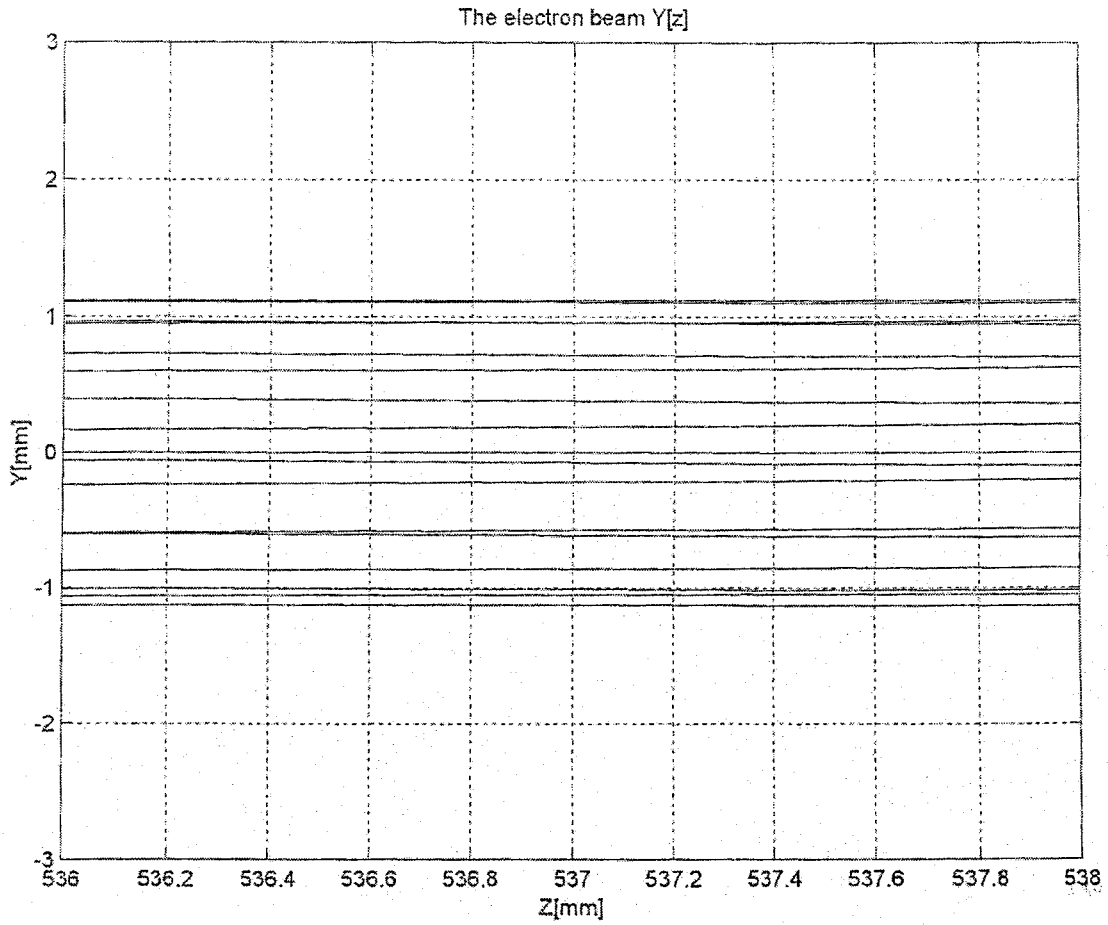

Fig. 7c: Wiggler's focus X – dimension at the wiggler exit

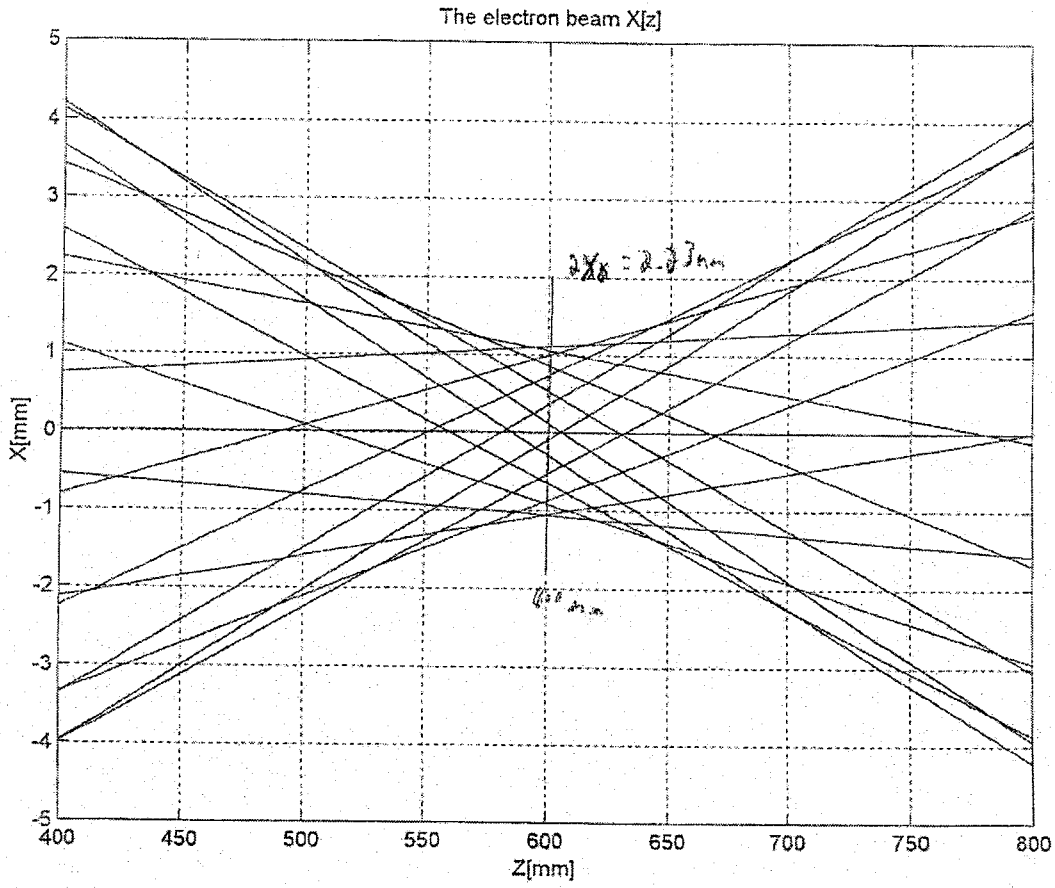

Fig. 7d: Larger scale (wiggler's focus)

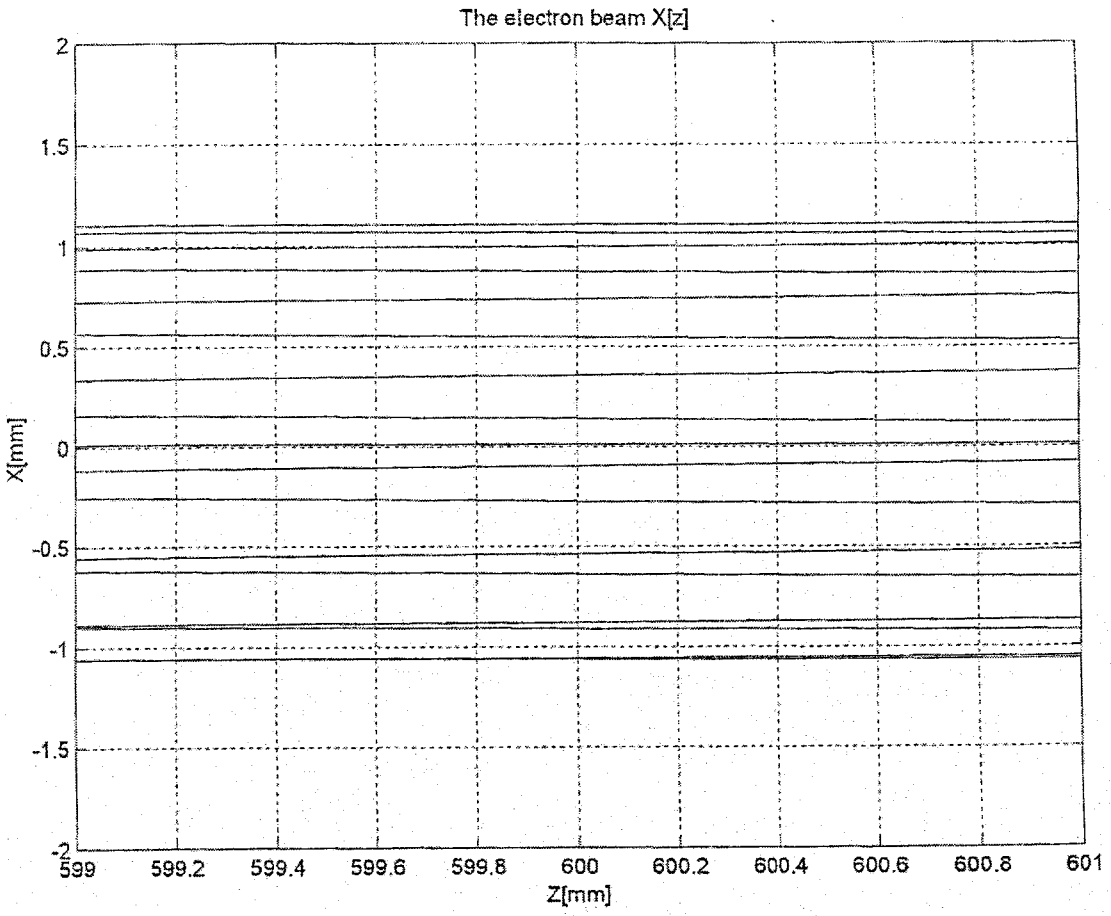

Fig. 7e: Wiggler's entrance (wiggler's focus)

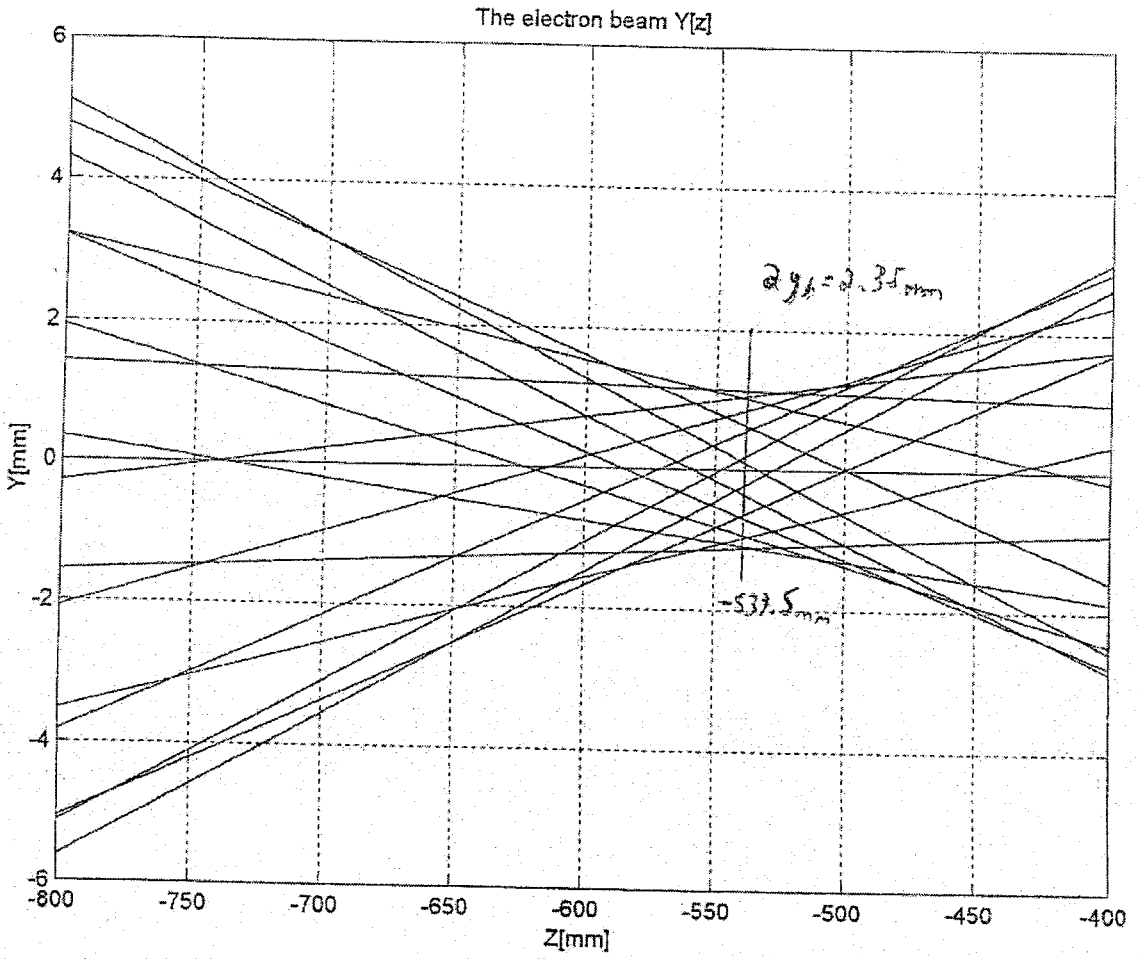

Fig. 7f: Wiggler's entrance (wiggler's focus)

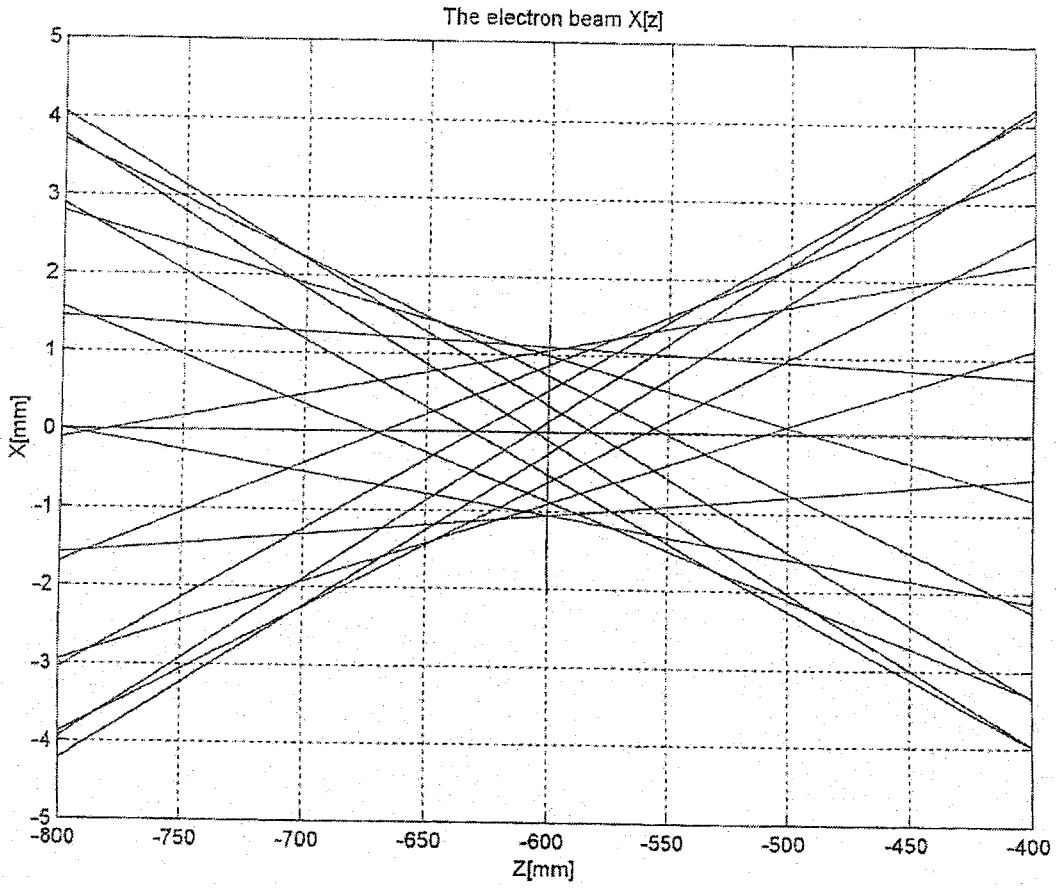

5. Finding the quad excitation current with Quad-Opt

We used the virtual waist parameters of the beam at the wiggler ends from the previous section.

We assumed (symmetrically) that the beam waist parameters before and after the quad sets was:

$Z_w = \pm 2680$ mm
$2W_{y0} = 2W_{x0} = 15$ mm

These assumptions are based on the experimental measurement of the beam spot on screen SC1 in previous runs. Of course these are only approximate values, and the assumptions that the beam had its waist on the screen is only an approximation.

With these assumptions, we operated "Quad-Opt", in order to find the quad excitation currents that image the waist before the quads to the virtual waists at the entrance to the wiggler (a symmetric solution is assumed to hold after the wiggler).

Tabel 4: Recommended Quadrupole Excitation Currents for transport of the e-beam across the terminal

Quad #	Solution 1	Solution 2
I_1	+ 1.56404A	- 1.63883A
I_2	- 1.19619A	+ 1.20707A
I_3	+ 1.30525A	- 1.30359A
I_4	- 0.65048A	+ 0.72489A
I_5	- 0.65048A	+ 0.72489A
I_6	+ 1.30525A	- 1.30359A
I_7	- 1.19619A	+ 1.20707A
I_8	+ 1.56404A	- 1.63883A

The two solutions of Quad-Opt are listed in Table 4. Only I_1- I_4 were calculated. $I_5 - I_8$ are the symmetric reflection of $I_1 - I_4$.

It is important to clarify what is meant by the current polarity sign. According to EL-OP programming assumption the quadrupole field configuration corresponding to I> 0 is shown in Fig. 8a.

Fig. 8a: Quadrupole field configuration corresponding to I> 0

The physical meaning of this assumption is that the magnetic field lines are oriented downward $B_y < 0$ when one measures them left of the center ($x > 0$) while facing downstream (+z direction): see EL-OP calculation of B_y of quad Q_1 for $I > 0$, $x > 0$ in Fig. 8b. This polarity convention fits the laboratory measurement of Jerzy (measured $B_x < 0$ for $y > 0$ under conditions of the control program definition: $I > 0$).

Because of the negative charge of the electron, one should expect that for the configuration of Fig. 8a (at $I > 0$) the Lorenz Force $-|e|\underline{V} \times \underline{B}$ will be directed towards the axis when the electron is off axis in the horizontal plane (namely – focusing in the horizontal – x dimension), and vice versa (defocusing) in the vertical (y) dimension.

A few notes are in order:

1. In Fig. 9a,b corresponding to solution 1 ($I_1 > 0$) there is first focusing by quad Q_1 in the x dimension (a) and defocusing in the y dimension, and vice versa in Figs. 10a,b corresponding to solution 2 ($I_1 < 0$). This is consistent with the field configuration of Fig. 8a.
2. As expected, the trajectories pictures of Fig. 9a (x dimension) is fully symmetric. However the picture of Fig. 9b (y dimension) is antisymmetric. We do not have yet clear explanation to this.
3. In comparing solution 1 (Fig. 9) to solution 2 (Fig. 10) we conclude that solution1 is preferable. The maximum expansion of the beam in solution 1 is in the y dimension:
   $(Y_b)_{max} = 25$ mm $\qquad (X_b)_{max} = 22.5$ mm
   The maximum expansion in solution 2 is also in the y dimension:
   $(Y_b)_{max} = 27.5$ mm $\qquad (X_b)_{max} = 21$ mm

   Considering that the vacuum tube has a circular cross section with I.D. = 66.4 mm, solution 1 is preferable and marginally satisfactory.

Fig. 8b: By for a positive displacement in x axis

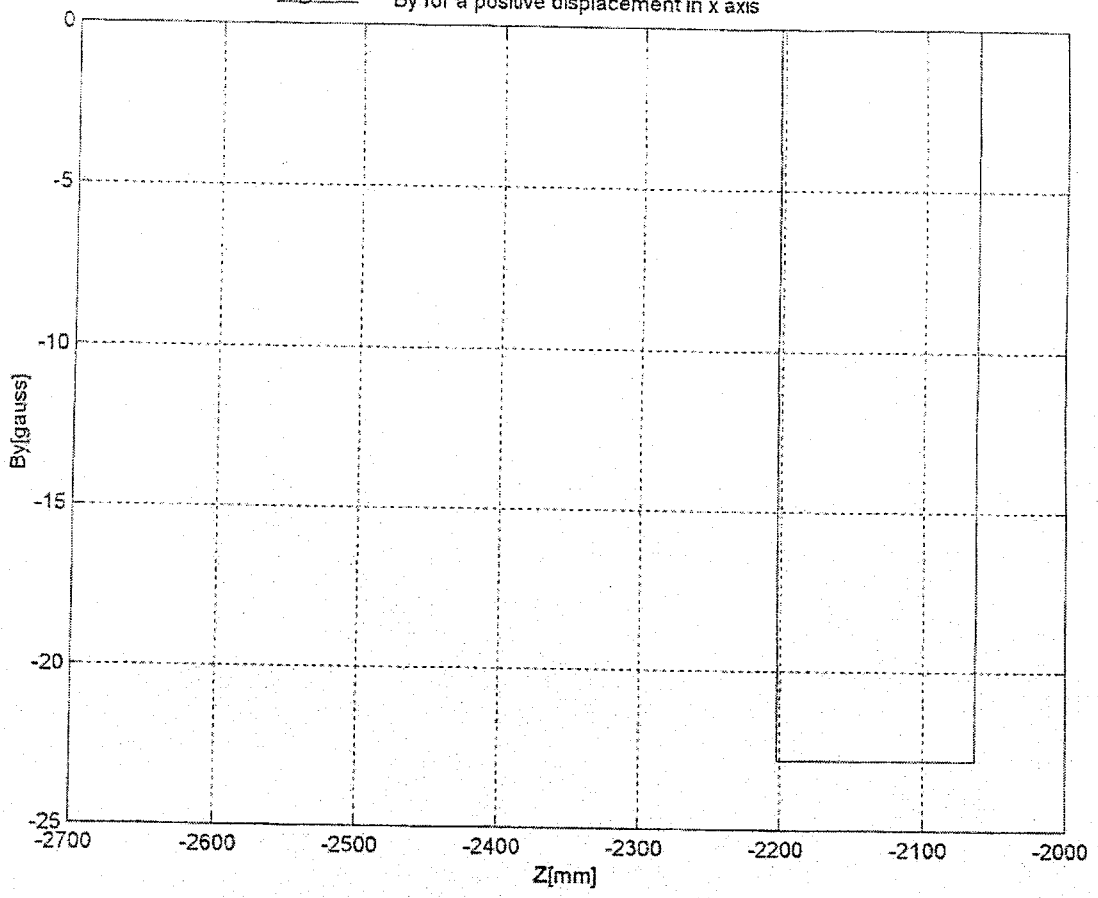

Fig. 9a: E-beam "all the way" for solution 1 x-dimension

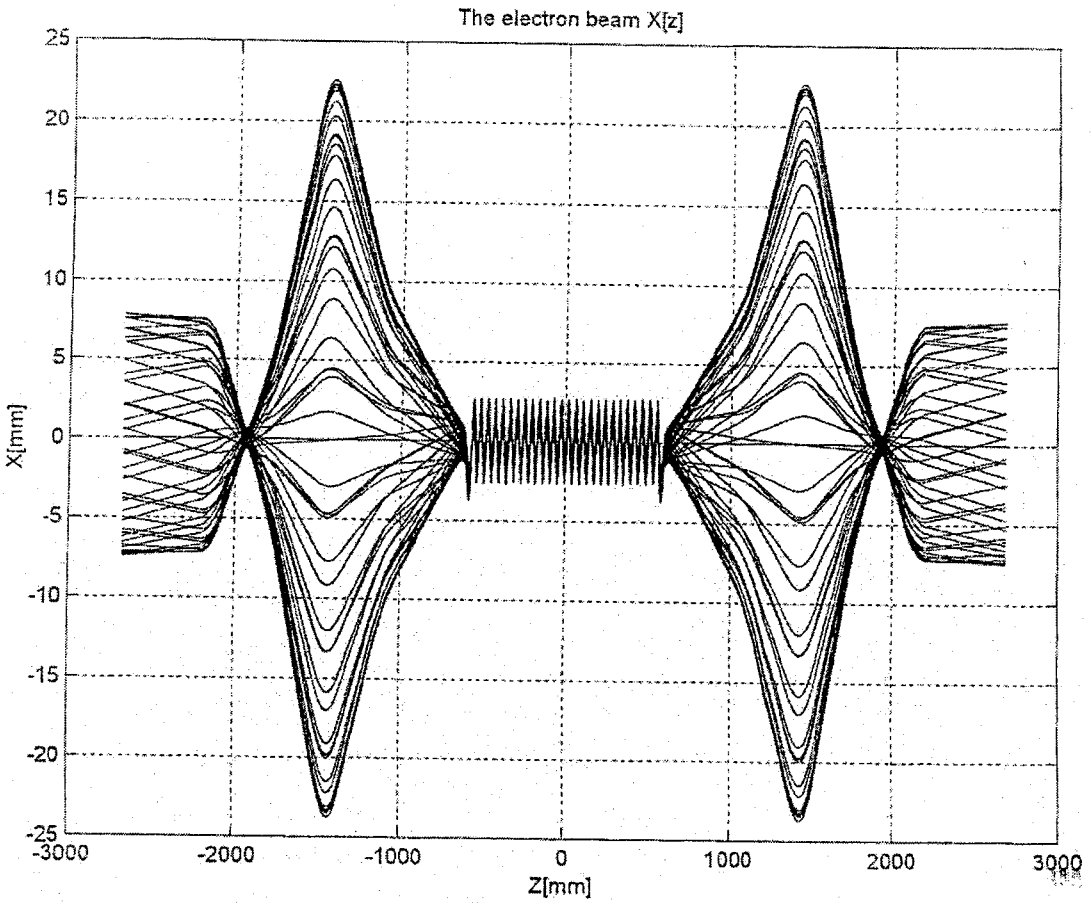

Fig. 9b: E-beam "all the way" for solution 2 y-dimension

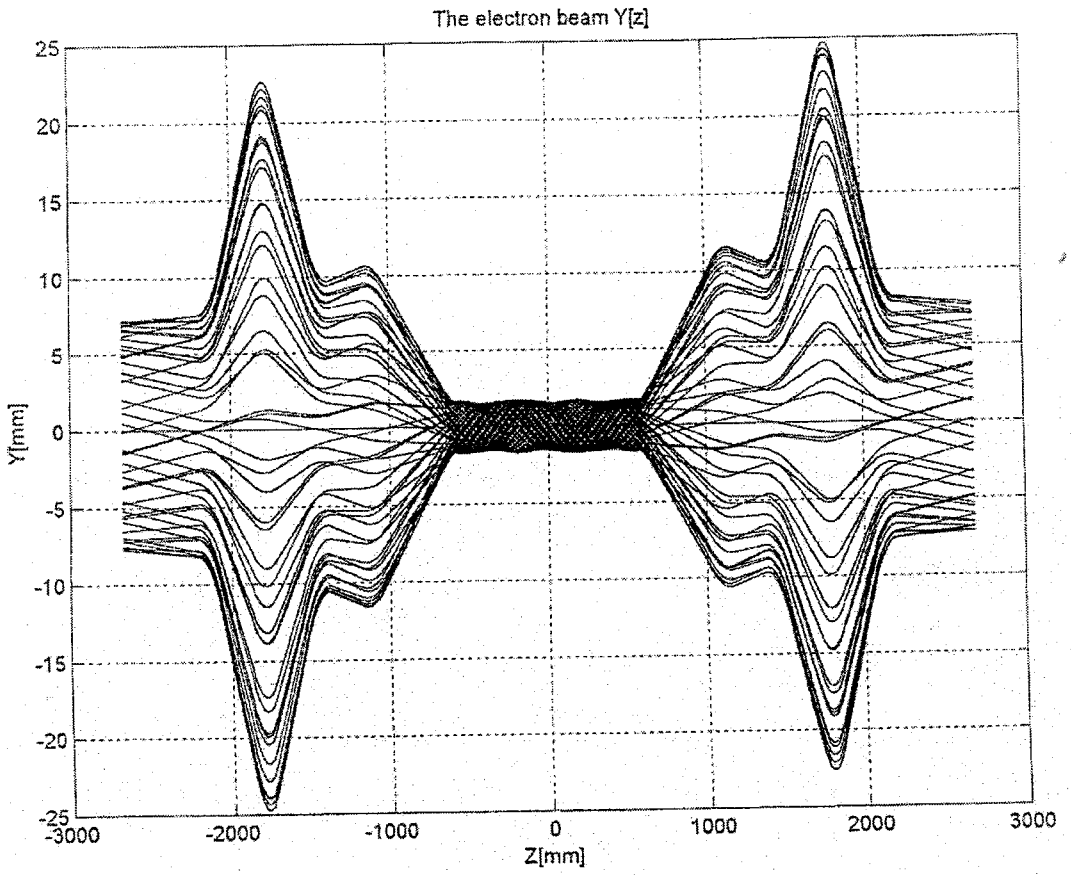

Fig. 10a: E-beam "all the way" solution 2

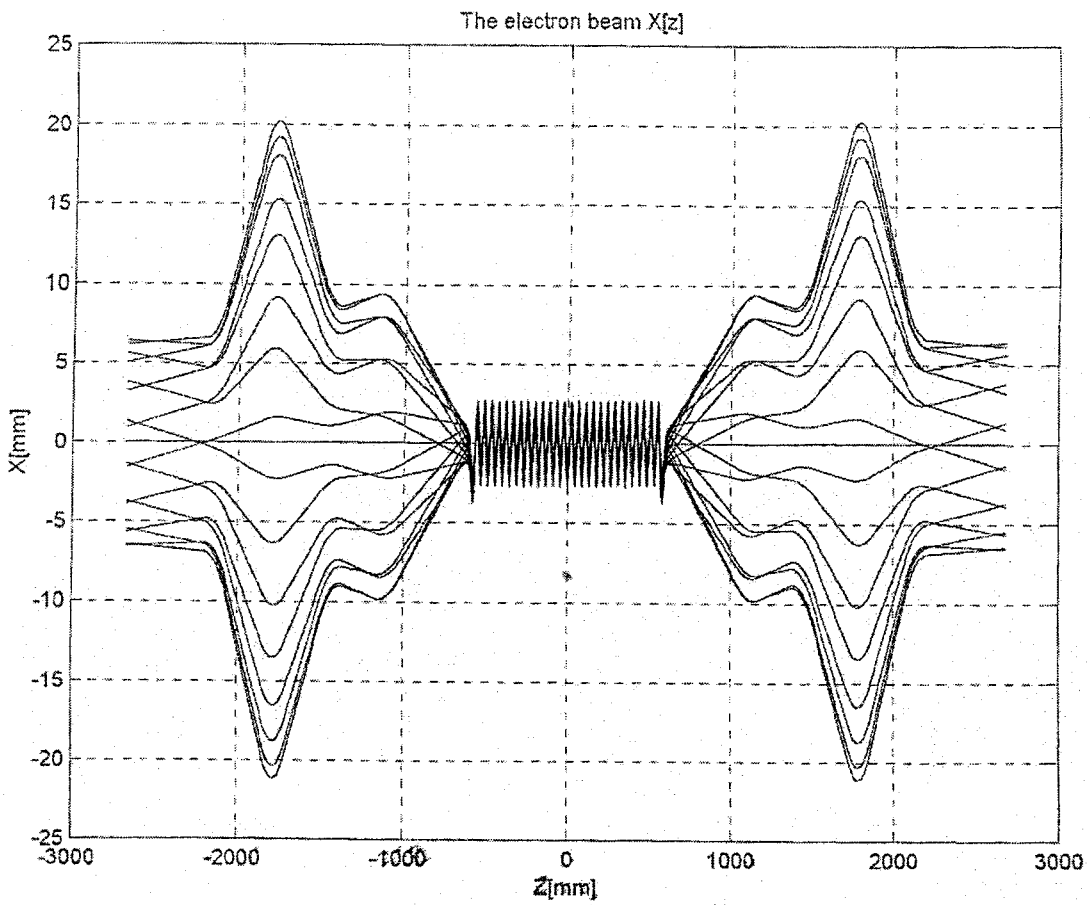

Fig. 10b: E-beam "all the way" solution 2

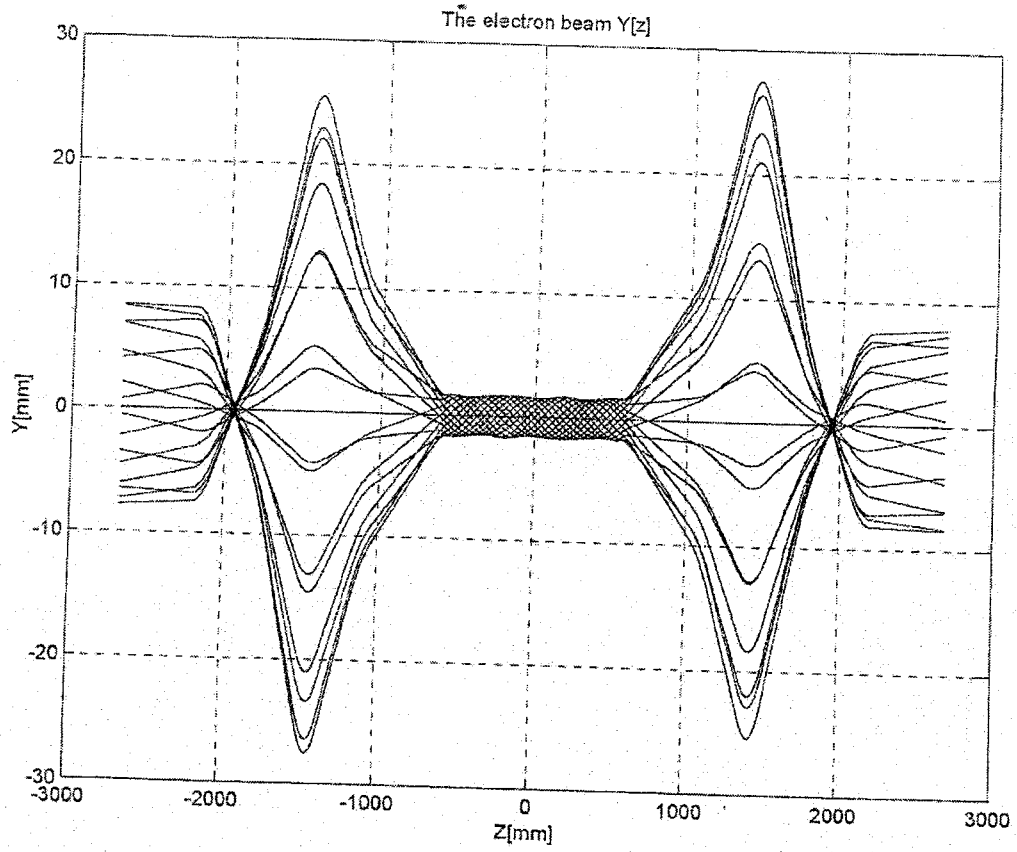

6. E-beam transport simulation "all the way"

The model assumptions of Quad-Opt and EL-OP are not identical. Quad-Opt relies on a paraxial ray approximation. EL-OP solves the exact force equations. In both cases, the quads are modeled by a "top-hat" model of uniform magnetic field.

To verify the validity of "Quad-Opt" solutions for the quad currents we operated EL-OP with the excitation currents of Table 4. The first set of simulations (Fig. 9,10) were carried out as before-starting at z=0 and going "all the way" (beyond the quads) forward and backward. The drawing show the combined data of the two runs. Fig. 9 displays solution 1 in the x(a) and y(b) dimensions. Fig. 10 displays solution 2 in the x(a) and y(b) dimensions. The initial conditions for the beam in these runs were:

$X_0 = -1.6466$ mm
$Y_0 = 0$
$\alpha_{x0} = 0$
$\alpha_{y0} = 0$
$R_{x0} = 1.00305$ mm
$R_{y0} = 1.574$ mm
$\alpha_{x0} = 21.93$ mrad
$\alpha_{y0} = 13.973$ mrad

These are the same conditions of scallop-free propagation in the wiggler (Fig. 6). Note that in Fig. 9 there are 59 particles in the simulation, while in Fig. 10 we only used 17.

For and additional test we ran EL-OP again with 17 particles, starting at a waist before the quads (after the acceleration tube): z = -2680 mm, going all the way beyond the quads to z = 2680mm. The results are shown in Fig. 11a,b (for solution1) and Fig. 12a,b (for solution 2). The initial conditions at z = -2680mm are:

$X_0 = 0$
$Y_0 = 0$
$\alpha_{x0} = 0$
$\alpha_{y0} = 0$
$R_{x0} = 7.5$ mm
$R_{y0} = 7.5$ mm
$\alpha_{x0} = 2.933$ mrad
$\alpha_{y0} = 2.933$ mrad

We note:

1. Contrary to the previous case, the beam trajectories pictures are symmetrical with respect to transformations $y \rightarrow -y$, but are not symmetric (or antisymmetric) with respect to transformation $z \rightarrow -z$. In the case of solution1 (Fig. 11 a,b) the maximum beam expansion in both x and y dimension is larger for $z > 0$ than for $z < 0$. In the other solution (Fig. 12a,b) – vice versa.
2. Excessive scalloping is observed in Fig. 12b. Indicates need for further checks.
3. Surprisingly the simulations of Fig. 11,12 suggest that solution 2 is preferable. They predict for solution 1 (Fig. 11) that the maximum expansion of the beam is at $z > 0$.
   $(y_b)_{max} = 28$ mm $\qquad$ $(x_b)_{max} = 28$ mm
   For solution 2 (Fig. 12a,b) the maximum expansion is at $z < 0$:

$(y_b)_{max}$ = 25 mm $(x_b)_{max}$ = 23 mm

4. There is still need to examine the consistency of the different simulations. Practically, it is recommended to try in the transport experiments current parameters around both solutions.

Fig. 11a: E-beam "all the way" for solution 1 starting at z = -2680 mm

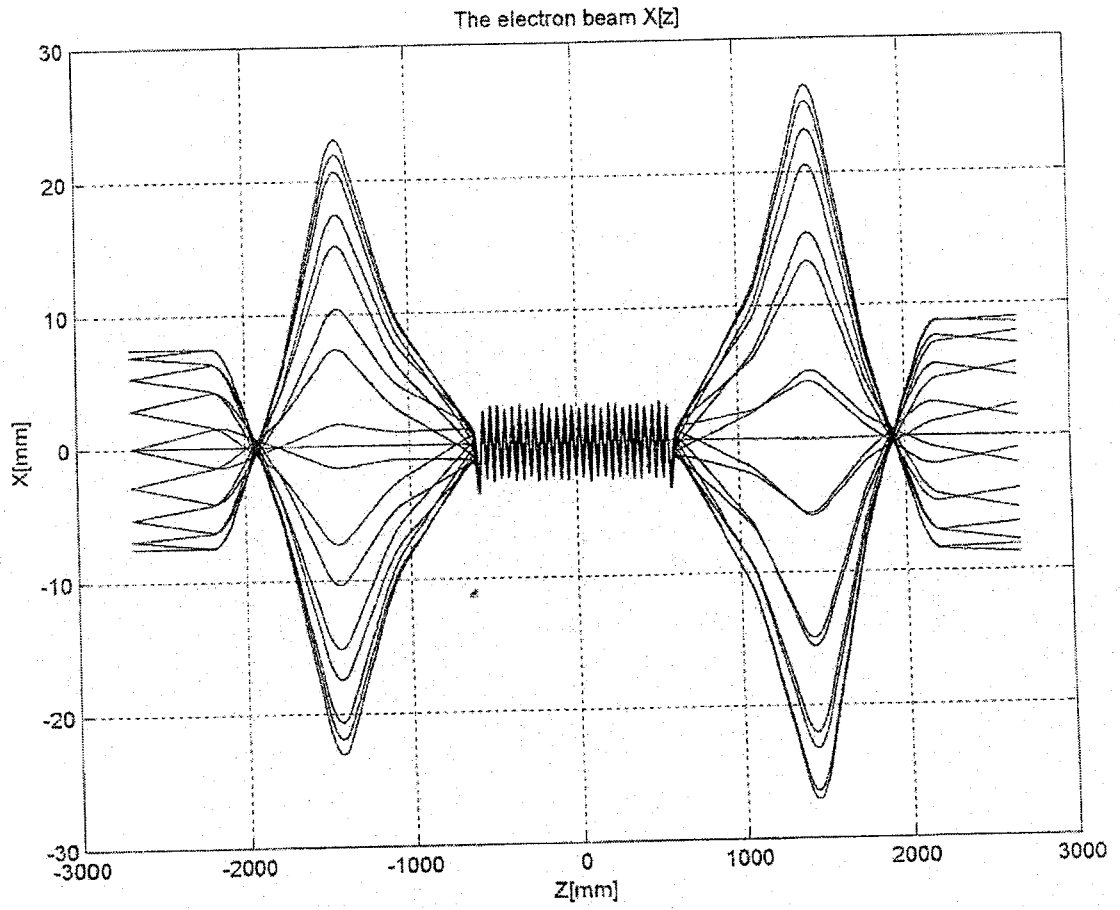

Fig. 11b: E-beam "all the way" for solution 1 starting at z = -2680 mm

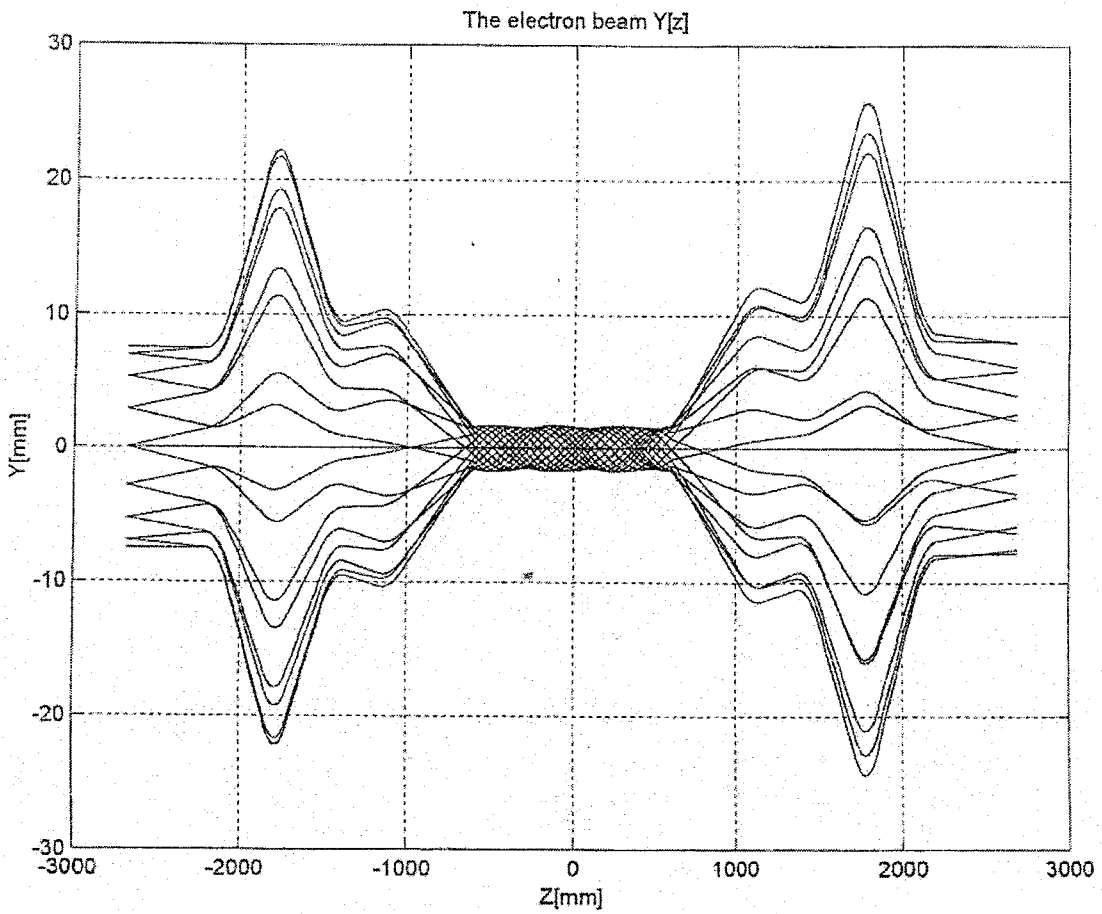

Fig. 12a: E-beam "all the way" for solution 2 starting from z = -2680 mm

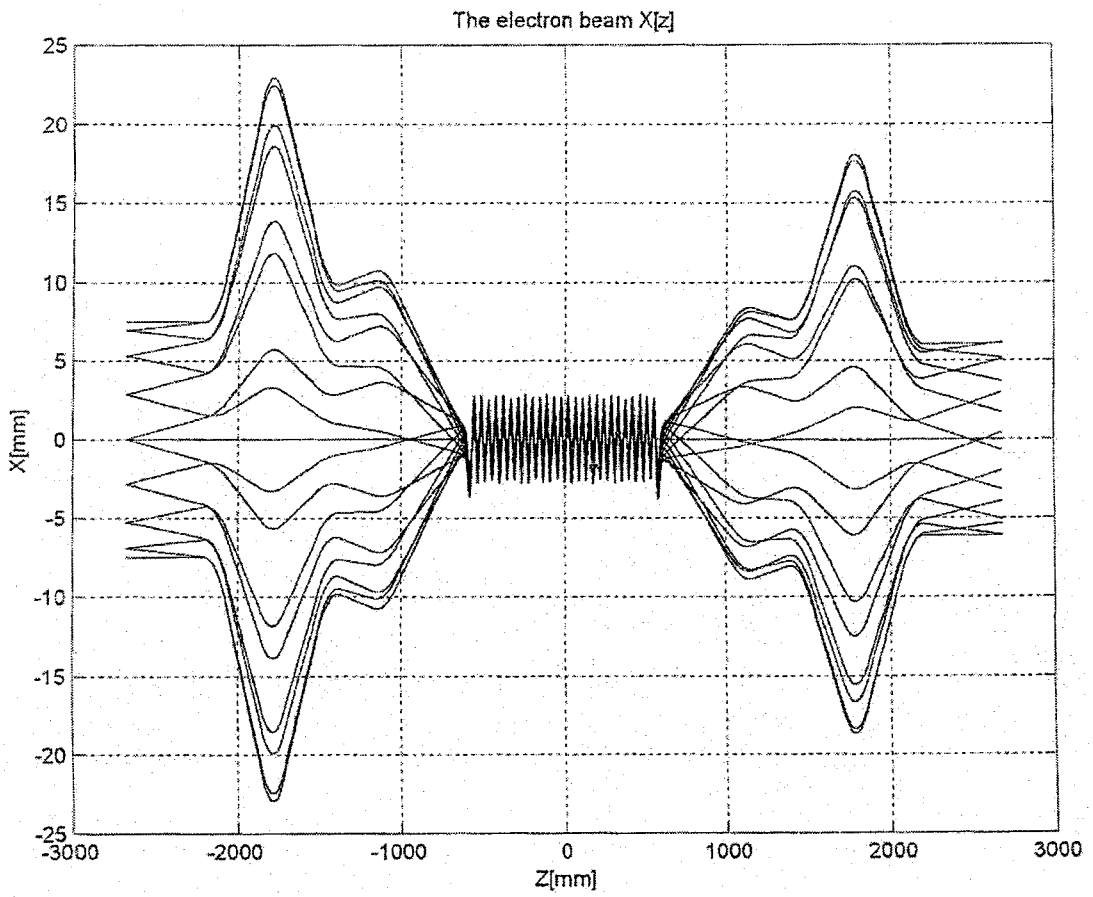

Fig. 12b: E-beam "all the way" for solution 2 starting from z = -2680 mm